Dimethyl Sulfide Photocatalytic Degradation in a Light-Emitting-Diode Continuous Reactor: Kinetic and Mechanistic Study

ARTICLE *in* INDUSTRIAL & ENGINEERING CHEMISTRY RESEARCH · JUNE 2011

Impact Factor: 2.59 · DOI: 10.1021/ie200297x

6 AUTHORS, INCLUDING:

Zimeng Wang
Stanford University
28 PUBLICATIONS **188** CITATIONS
SEE PROFILE

Yuancan Dai
Fudan University
2 PUBLICATIONS **46** CITATIONS
SEE PROFILE

Shicheng Zhang
Fudan University
81 PUBLICATIONS **1,558** CITATIONS
SEE PROFILE

Jian-Min Chen
Fudan University
166 PUBLICATIONS **2,683** CITATIONS
SEE PROFILE

I&EC research
Industrial & Engineering Chemistry Research

ARTICLE

pubs.acs.org/IECR

Dimethyl Sulfide Photocatalytic Degradation in a Light-Emitting-Diode Continuous Reactor: Kinetic and Mechanistic Study

Zimeng Wang,[†,‡] Jing Liu,[‡] Yuancan Dai, Weiyang Dong, Shicheng Zhang,* and Jianmin Chen*

Department of Environmental Science and Engineering, Fudan University, Shanghai 200433, China

ABSTRACT: This study investigated the feasibility, kinetics, and reaction pathways of the photocatalytic degradation of dimethyl sulfide (DMS) in a light-emitting-diode- (LED-) based continuous reactor. Four types of LEDs, with peak wavelengths at 365, 375, 385, and 402 nm, were used for comparison. The data were fitted with the Langmuir−Hinshelwood kinetic model, in which the rate constants for 365- and 375-nm LEDs were significantly larger than those for the 385- and 402-nm LEDs. The effect of wavelength on the reaction rate followed the TiO_2 absorption spectrum. The effect of radiation intensity agreed with a nonlinear power law and was attributed to the TiO_2 absorption of photon energy. For the 365- and 375-nm LEDs, the transition of the exponent values from first-order to one-half-order was estimated to occur at 0.5−1.0 $mW \cdot cm^{-2}$, whereas the 385- and 402-nm LEDs did not show a transition at this intensity. Dimethyl sulfoxide (DMSO), dimethyl sulfone ($DMSO_2$), dimethyl disulfide (DMDS), methanethiol (MT), methanesulfonic acid (MSA), and sulfate were identified as the reaction products by gas chromatography (GC), gas chromatography−mass spectrometry (GC−MS), and ion chromatography (IC). A plausible reaction mechanism is proposed for DMS photocatalytic degradation based on the reaction products detected and possible intermediates formed.

1. INTRODUCTION

The emission of odorous pollutants from wastewater treatment plants, landfills, livestock facilities, and paper production plants presents serious environmental and health concerns. Many of the emitted species are highly disagreeable and toxic. Dimethyl sulfide (DMS) is a representative odorous compound emitted during various anaerobic decay processes.[1] Although there are natural sources of DMS, mainly from oceanic phytoplankton,[2] anthropogenic emissions of DMS have commonly been detected in paper pulping[3] and wastewater treatment[4] processes. DMS has a very low odor threshold value of 0.6−40 ppb and is an irritant to the eyes, skin, and respiratory system. Repeated exposure to DMS (1 ppm) can lead to chronic respiratory and cardiovascular diseases.[5] Some abatement technologies have been developed, such as activated carbon adsorption, activated sludge, chemical scrubbing, and incineration. To some extent, however, these techniques encounter the limitations of being nondestructive and/or expensive because of intensive energy and/or material (chemical and/or water) consumptions.[6] Although biofiltration is destructive and cost-effective, it is limited by overgrowth of biomass, strict humidity requirements, and incomplete conversion.[7]

Semiconductor-mediated heterogeneous photocatalysis has become a promising and intensively studied technology for the abatement of organic gaseous pollution, which can be carried out at ambient temperatures without extra addition of oxidant chemicals.[8] However, the photocatalytic degradation of odorous reduced sulfur pollutants in the gas phase is much less documented.[9−11] In addition, most existing photocatalytic studies were conducted using germicidal lamps (UV-C, 254 nm) and fluorescent black-light lamps (300−370 nm).[12] However, these traditional UV sources are limited by shortcomings related to sustainability and the environment, such as energy inefficiency and mercury pollution.[13] Light-emitting-diodes (LEDs) offer a promising replacement for conventional light sources in many applications. The advantages of LEDs include high energy efficiency (little heating), long lifetime, and the availability of monochromatic irradiation. In engineering practice, the compact size and DC power supply of LEDs offer greater flexibility for field use. The successful commercialization of UV-LEDs also enables their application in the semiconductor-mediated photocatalytic decomposition of organic pollutants. Recently, some studies have exploited LEDs as light sources for the photocatalytic degradation of aqueous pollutants, such as perchloroethylene (PCE),[13] Reactive Red,[14] *o*-cresol,[15,16] and methylene blue.[17] A few other studies constructed LED-based photocatalytic microreactors,[18] water purifiers,[19] and sterilizers[20] or exploited the near-monochromatic property of visible-light LEDs to develop dye-photosensitizer-based reactors.[21−25] The results have demonstrated that LEDs represent a practical and competitive alternative light source for photocatalysis applications.[17,22,26]

Nevertheless, to the best of our knowledge, very few reports have been published so far about the LED-based photocatalytic degradation of gaseous odorous pollutants. Also, no systematic study on the effects of LED wavelength and intensity on photocatalytic degradation processes has been reported. Several groups have investigated the rate and products of DMS photocatalytic oxidation and the effects of ozone, humidity, and catalyst deactivation.[9,27,28] However, the kinetics and mechanism have not been studied for a wide range of irradiation parameters. Therefore, our objective in this work was to assess the feasibility and kinetics of the photocatalytic degradation of DMS in a flow-through planar film reactor under varied LED illuminations.

Received: February 11, 2011
Accepted: May 23, 2011
Revised: May 17, 2011
Published: May 23, 2011

dx.doi.org/10.1021/ie200297x | *Ind. Eng. Chem. Res.* 2011, 50, 7977–7984

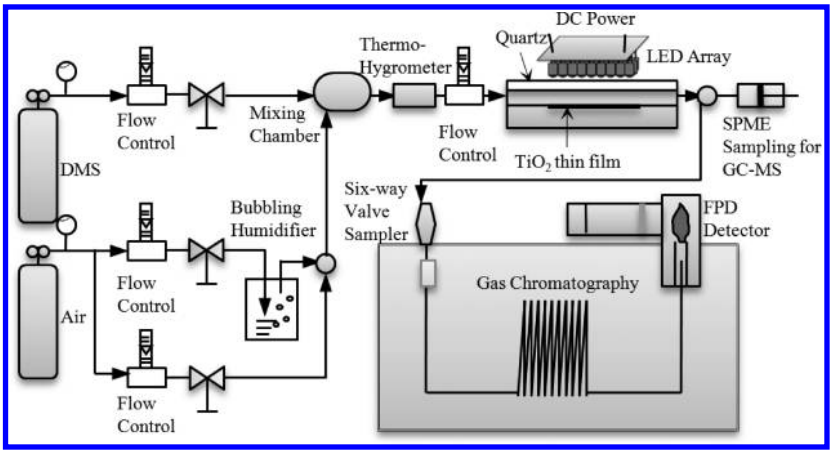

Figure 1. Schematic diagram of the experimental setup for the photocatalytic degradation of dimethyl sulfide in an LED-based continuous reactor.

This study also intended to gain insight into the effects of wavelength and intensity on the reaction rate. Based on the identification of the reaction products, possible photocatalytic degradation pathways are also discussed.

2. EXPERIMENTAL SECTION

2.1. Chemicals and Photocatalyst Preparation. Dimethyl sulfide gas with a traceable concentration of 50 ppmv in pure nitrogen was supplied by Shanghai Qingkuan Company and used as the odorous gas source. A commercial TiO_2 photocatalyt (P25) was provided by Degussa AG Company; it contained 20% rutile and 80% anatase with a primary particle size of 50 nm and a specific surface area of 50 $m^2 \cdot g^{-1}$. Immobilization of TiO_2 particles was performed by impregnating a glass plate in a TiO_2 aqueous suspension. A P25 suspension of 4 $g \cdot L^{-1}$ concentration was prepared at pH 3 in deionized water and ultrasonicated for 1 h prior to the dip-coating. The plate was withdrawn vertically at a constant speed of 20 $mm \cdot min^{-1}$ by an electrical hoister. The coated plate was air-dried and heated in an oven at 200 °C for 4 h. The dip-coating process was repeated several times to increase the catalyst loading. This method has been shown to reproducibly prepare fine TiO_2-coated glass plates.[29] The coated area of the plate was 2.5 cm × 6.0 cm. The actual loading of TiO_2 film after nine dip-coating cycles was 36.3 $mg \cdot cm^{-2}$. The coated plate was then fixed in a homemade photoreactor.

2.2. Photoreactor and Experimental Setup. Figure 1 shows the schematics of the photoreactor and experimental setup. A water-bubbling humidifier and a thermohygrometer (ColliHigh, Beijing, China) were used to adjust and monitor the relative humidity of the gas mixture. The DMS gas and humidified air were mixed in a Teflon chamber (300 mL) before entering the photoreactor. The flow rates of both gases were manipulated to prepare the desired DMS concentration and humidity in the experiments. The photoreactor was made of polytetrafluoroethylene (PTFE, or Teflon), to minimize gas adsorption onto the reactor surfaces. A groove with the specific dimensions of the glass plate was made to house the catalyst film, and thus, only one side of the plate was effective. A gas flow channel was made between the catalyst film and the quartz plate, which served as the top cover of the reactor. The flow passage was 5 mm in height, and the effective volume of the reactor was 7.5 mL.

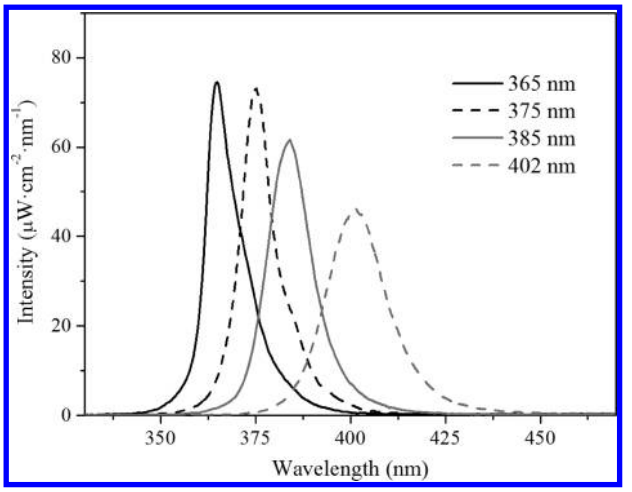

Figure 2. Emission spectra of four LED arrays obtained at an average intensity of 1.0 $mW \cdot cm^{-2}$ by setting the voltage at 3.47, 3.37, 3.26, and 3.33 V for the 365-, 375-, 385-, and 402-nm LEDs, respectively.

2.3. LED Characterization. The LEDs used in this work were p−n junction devices made of indium gallium nitride. They were designed as 3 × 9 LED arrays of individual LED lamps (Yuan-Chuang Electronic, Shenzhen, China). Four different types of LEDs were used. As shown in Figure 2, the emitting spectra of the four LED arrays were measured with a spectroradiometer (International Light, Peabody, MA). The peak wavelengths of the four LEDs were 365, 375, 385, and 402 nm, and their half height widths were around 10 nm, except for the 402-nm LED (18 nm). The directivity of these LEDs was 20° for 50% of the total irradiation energy. The LED arrays were fixed at a distance of 3.5 cm directly above the catalyst film. The light intensity projected onto the catalyst film was determined by averaging 20 measurements at varying positions on the plate. The standard deviation of the measured light intensities was within ±20%, indicating a relatively uniform irradiation field. The LED irradiance increased with the DC voltage applied to the LED array, so the light intensities were adjusted from 0.5 to 2.5 $mW \cdot cm^{-2}$ by manipulating the input voltages (less than 4 V).

2.4. Experimental Procedure and Product Detection. The experiments were conducted at room temperature (22 ± 2 °C). The relative humidity of the gas mixtures in the reactor was controlled at (22 ± 2)%, at which the highest conversion of DMS

was reported in a previous study.[9] Before each experiment, the inlet DMS concentration was monitored by gas chromatography (GC), and the reactor was pre-equilibrated with a flow of the gas mixture for at least 30 min until the inlet and outlet DMS concentrations became equal. Then, the LED array was turned on. Effluent gas was sampled periodically by a six-way valve and measured by gas chromatograph (Haixin GC-930, Shanghai, China; Agilent HP-PLOT Q Column) with a flame photometric detector (FPD). Approximately 30 min after the light was turned on, the effluent concentration decreased rapidly with time and finally became stable. The system was considered to have reached steady state when four consecutive GC measurements in 1 h gave DMS concentrations within 5% deviation. The typical duration of each experiment was around 2 h. The reactant DMS and possible intermediates were identified by comparing their GC retention times to those of pure compounds and also by analyzing the effluent gas with a gas chromatography−mass spectrometry (GC−MS) system (Agilent 6890 GC/6973N MS). An Agilent HP-5MS column and a Varian VF-wax capillary column were used to detect the nonpolar and polar compounds, respectively, in the effluent products. Given the trace concentrations of the reaction products, the GC−MS gas samples were collected using a solid-phase microextraction (SPME) technique. A Supelco SPME fiber [polydimethylsiloxane (PDMS)/Carboxen] was used to enrich the effluent sample for 10 min, and the sample was then injected immediately into the GC−MS instrument. Mass spectra were searched and matched using the NIST database, and the spectra were assigned to the corresponding compounds if they had at least 90% similarity to the reference spectra. The catalyst plate after reaction was ultrasonicated in deionized water for 1 h, and then the solution was filtered with a 0.45-μm membrane. The products in the filtrate were identified by ion chromatography (Dionex ICS 3000, IonPacAS11 column and ED50 conductivity detector).

3. RESULT AND DISCUSSION

3.1. Conversion and Reaction Rate. Assuming a negligible pressure drop along the reactor, the conversion yield, X, in the reactor is given by[30]

$$X = \frac{C_{in} - C_{out}}{C_{in}} \times 100\% \quad (1)$$

where C_{in} and C_{out} are the steady-state DMS concentrations measured at the reactor entrance and exit, respectively. Although intrinsic kinetic measurements are usually normalized by the quantity of the catalyst (mass or specific surface area), in many literature reports and in engineering practice, the heterogeneous photocatalytic reaction rate on an immobilized catalyst is expressed in terms of the apparent surface area of the catalyst support. The reaction rate r ($mol \cdot s^{-1} m^{-2}$) was calculated based on the mass balance[30−32]

$$r = \frac{Q(C_{in} - C_{out})}{S} \quad (2)$$

where Q is the volumetric flow rate ($m^3 \cdot s^{-1}$) and S is the catalyst support surface area (15 cm^2). In this calculation, r is a measurement of the average rate of the reaction in the reactor normalized by the area of the catalyst film under specific conditions, rather than an intrinsic reaction rate for use in any kinetic model.

Catalyst-free and irradiation-free control experiments were conducted to exclude any possible transformation of DMS other than photocatalytic degradation induced by TiO_2. Photolysis of DMS is a possible transformation pathway under UV light,[33,34] but there was no detectable degradation in all catalyst-free control experiments. This result can be attributed to the negligible absorption of DMS (adsorption peak at 210 nm[35]) of the photon energy for $\lambda > 300$ nm.

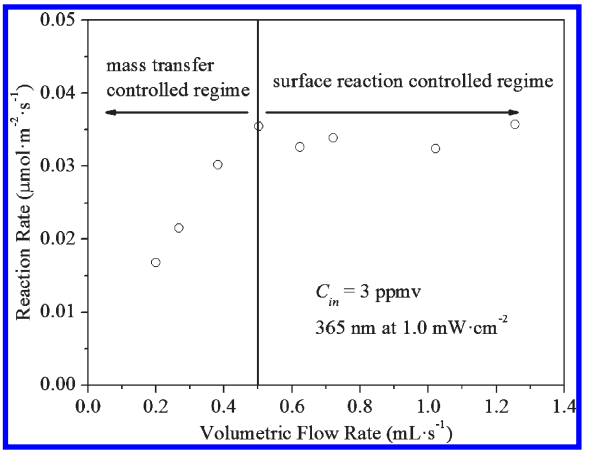

Figure 3. DMS reaction rates measured at different volumetric flow rates (C_{in} = 3 ppmv, 365-nm LED at 1.0 mW·cm^{-2}).

3.2. Effect of Mass Transfer. In flow-through photocatalytic reactors, mass transfer can play a role in the overall behavior of the reaction rate.[36] Intraparticle mass-transport resistance is negligible because of the thin-film configuration and light penetration limitation, so only bulk transport and surface reaction kinetics determine the observed reaction rate. As the flow rate increases, the reaction rate should become independent of the fluid velocity, indicating that the reaction kinetics is free of mass-transfer limitations and is dominated by the surface reactions. The dominant regime depends on the flow behavior of the gas mixture and the experimental conditions. Figure 3 presents the experimental DMS degradation reaction rate as a function of the volumetric flow rate under constant conditions of inlet concentration and radiation. It shows two reaction regimes, which is consistent with other studies of continuous gas-phase photocatalytic reactors using immobilized catalysts.[36−40] Mass-transfer limitations were present at flow rates below 0.5 mL·s^{-1} (Re < 2.75), whereas the surface-reaction-kinetics-controlled regime was achieved at higher flow rates (residence time < 15 s). Consequently, the subsequent experiments to evaluate the intrinsic photocatalytic activity were carried out at flow rates where the effect of mass transfer was small.[41]

3.3. Langmuir−Hinshelwood Model. The Langmuir−Hinshelwood (L−H) model is widely applicable for the photocatalytic oxidation kinetics of volatile organic compounds (VOCs). The assumption in this model is that the degradation follows a rate-limiting step in which a surface-adsorbed molecule reacts with a reactive species (e.g., hydroxyl radical). At steady state, the concentration of these transient reactive oxidants can be assumed to be constant, so that the reaction rate is proportional to the surface coverage of the VOC molecules. Adapting a simple Langmuir isotherm for VOC adsorption, the reaction rate is given by the equation[42,43]

$$r = k\frac{KC_S}{1 + KC_S} \quad (3)$$

where K ($m^3 \cdot mol^{-1}$) is the Langmuir adsorption constant; C_S ($mol \cdot m^{-3}$) is the gaseous concentration near the catalyst

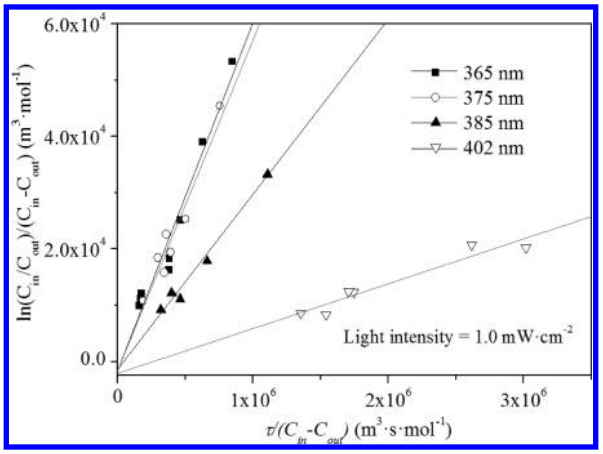

Figure 4. Langmuir−Hinshelwood model fitting results in a continuous reactor for four types of LEDs at a constant light intensity of 1.0 mW·cm^{-2}. The ranges of experimental conditions were as follows: inlet DMS concentration = 0.5−4.0 ppmv, residence time = 5−15 s.

Table 1. Langmuir−Hinshelwood Kinetic Model Parameters for Four Types of LEDs Obtained at 1.0 mW·cm^{-2}

wavelength (nm)	k (mol·m^{-2} s^{-1})	K (m^3·mol^{-1})	R^2
365	1.93×10^{-7}	1602.9	0.956
375	1.84×10^{-7}	1594.9	0.942
385	1.12×10^{-7}	1390.1	0.983
402	1.90×10^{-8}	2101.2	0.926

surface; and k (mol·m^{-2}·s^{-1}) is a rate constant, which is a function of temperature, light flux, and catalyst properties.

In a flow-through reactor at steady state, there is a concentration gradient of C_S along the length of the reactor. When the bulk transport limitation is small, the flow pattern in the reactor can be approximately described by the plug-flow model, which is given by the integral equation[30,44−46]

$$\frac{\tau}{h} = \frac{C_{in}S}{F} = \int_{C_{out}}^{C_{in}} \frac{dC_S}{r} = \int_{C_{out}}^{C_{in}} \frac{dC_S}{\left(\frac{kKC_S}{1+KC_S}\right)}$$

$$= \frac{K(C_{in} - C_{out}) + \ln(C_{in}/C_{out})}{kK} \quad (4)$$

where τ is the residence time (s), h is the thickness of reactor volume (5 mm), and the left-hand side can be analogously defined as a "surface time". F (mol·s^{-1}) is the molar feed rate at the entrance to the reactor. The two parameters K and k can be obtained by linear fitting of a plot of $\ln(C_{in}/C_{out})/(C_{in} - C_{out})$ versus $\tau/(C_{in} - C_{out})$ from experimental data.

By manipulating the inlet DMS concentration and residence time, kinetic data were collected at 1.0 mW·cm^{-2} intensity for the four LED arrays. Figure 4 shows the experimental data obtained using the four types of LEDs, which are in good agreement with the integral rate law analysis. Table 1 summarizes the kinetic parameters of the photocatalytic degradation reaction for four types of LEDs. The order of the rate constants k for the four types of LED was found to be 365 nm > 375 nm > 385 nm > 402 nm, and the values for the latter two LEDs were significantly smaller than those for the former two. At the low DMS concentrations used in this study, the L−H model predicted

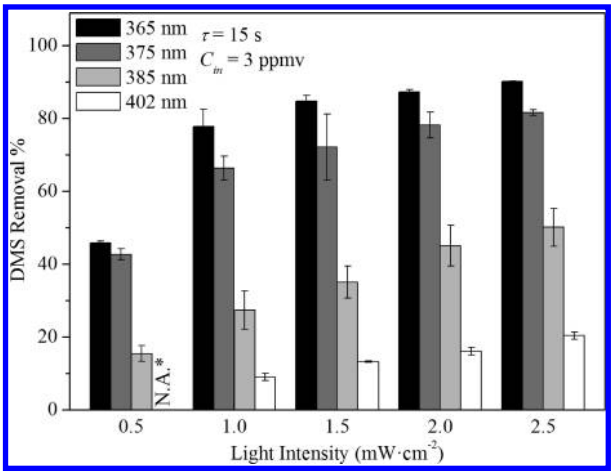

Figure 5. Effects of light intensity and wavelength on the DMS conversion efficiency (C_{in} = 3 ppmv, τ = 15 s). The error bars represent the standard deviations of duplicate measurements. Note that the 0.5 mW·cm^{-2} data for the 402-nm LED are not available (N.A.) because of the DC voltage limitation of the lamp.

that the reaction rate was proportional to the concentration of DMS with a proportionality constant of kK.

3.4. Effects of Light Wavelength and Intensity. To understand the effects of light wavelength and intensity on the reaction rate, experiments were conducted in the surface-kinetics-controlled regime (C_{in} = 3 ppmv, τ = 15 s) using four types of LEDs at various light intensities from 0.5 to 2.5 mW·cm^{-2}. The data on DMS removal efficiency (Figure 5) showed that, at the same light intensity, the 365-nm LED had the highest removal efficiency (up to 90% at 2.5 mW·cm^{-2}), although the 375-nm LED, which is much cheaper than the 365-nm one, also showed competitive performance. The 385- and 402-nm LEDs exhibited lower removal efficiencies. It should be noted that this short residence time (15 s) was chosen to minimize mass-transfer limitations. At lower flow rates, more complete conversion of DMS could be expected. These results demonstrate that the UV-LED photocatalytic process could be a good alternative technique for deodorization.

The data were also interpreted in terms of DMS reaction rate (Figure 6). It is believed that the variation of the reaction rate as a function of the wavelength of the incident irradiation generally follows the absorption spectrum of the catalyst, with a threshold corresponding to its band gap energy (E_g).[47] Even though the LED spectra overlapped to some extent, the reaction rate versus wavelength relationship still resolved a good agreement with the absorption spectrum of P25 TiO_2, with a threshold indicating the band gap energy (for P25 TiO_2, E_g = 3.2 eV, and $\lambda_{threshold}$ = 380 nm). This phenomenon can be attributed to the photon-inducing nature of the heterogeneous photocatalytic process.

Photon energy is an important factor that affects the photocatalytic reaction rate. Theoretical kinetic derivations[47,48] and experimental studies[43,49,50] have shown that photocatalytic reactions can occur in several regimes in association with light intensity. At low intensity, the reaction rate is proportional to the intensity I; at intermediate intensity, the rate varies as $I^{0.5}$; and at sufficiently high intensity, the reaction rate becomes a constant independent of light intensity and limited only by mass transfer. This transition is attributed to the fact that increased intensity enhances the electron−hole recombination process (which is second-order) faster than the oxidation process (which is pseudo-first-order in excited oxidant).[47,51]

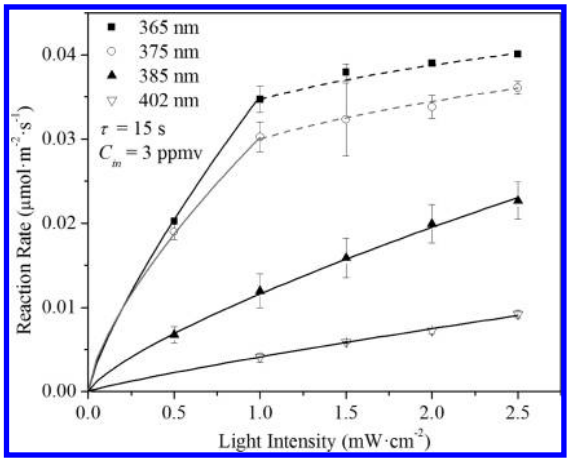

Figure 6. Effects of light intensity and wavelength of four LEDs on the reaction rate of DMS (C_{in} = 3 ppmv, τ = 15 s). The error bars represent the standard deviations of duplicate measurements.

Table 2. Fitting Results of the Nonlinear Power Relationship between Light Intensity and Reaction Rate

wavelength (nm)	fitting range I (mW·cm^{-2})	r' (mol·m^{-2}·s)	α
365	0−1.0	3.51×10^{-8}	0.78
	1.0−2.5	3.47×10^{-8}	0.16
375	0−1.0	3.02×10^{-8}	0.69
	1.0−2.5	3.00×10^{-8}	0.20
385	0−2.5	1.16×10^{-8}	0.75
402	0−2.5	4.12×10^{-9}	0.86

A nonlinear power law was observed in experiments[36,43] and implemented in a modified L−H kinetic model[38,46] to account for the effect of light intensity

$$r = r'I^{\alpha} = \frac{kKC_S}{1 + KC_S} I^{\alpha} \quad (5)$$

where r' is the reaction rate independent of light intensity. The exponent α varies from 1 to 0 as light intensity increases and can be estimated by a nonlinear fitting of the experimental data, as shown in Figure 6. For the 365- and 375-nm LEDs, the effect of light intensity could be divided into two regimes. At sufficiently weaker levels of intensity (<1.0 mW·cm^{-2}), the reaction rates were nearly first-order in the light intensities, whereas at higher intensities, the curves of intensity versus reaction rate dramatically leveled off.

Piecewise-fitting results (Table 2) showed significant differences in the α values obtained at low intensity (<1.0 mW·cm^{-2}) and high intensity (1.0−2.5 mW·cm^{-2}). Consequently, the transitions were estimated to occur at 0.5−1.0 mW·cm^{-2}. At high intensity, the α values from the fitting results were less than 0.5. Such a result was also reported in previous studies and can be partially explained in terms of excessive generation of hydroxyl radicals (OH$^{\bullet}$) at high intensity leading to faster self-recombination.[46,52] External transport could also start to play a role in this regime. At even higher intensities, the reaction rates would be expected to achieve plateaus where the system became completely mass-transfer-limited. On the other hand, there were no obvious transitions in the α values around 0.5−1.0 mW·cm^{-2} for the 385- and 402-nm LEDs, and α values larger than 0.5 could fit the entire light intensity range up to 2.5 mW·cm^{-2}. The transition points vary with each application depending on the catalytic configuration and flow pattern,[51] and the different behaviors of the 385- and 402-nm LEDs should be attributed to the weaker absorption of photon energy by TiO_2. Different values of the exponent α were also observed in experiments comparing anatase and rutile TiO_2, which have different absorptions of photon energy.[48] Our results based on LED photocatalysis are consistent with a previous report[49] that 1-sun equivalent illumination level is often observed as the transition point between the first-order and one-half-order regimes, and the sun emits about 1−2 mW·cm^{-2} for wavelengths below 350 and 400 nm, according to the terrestrial solar spectrum.

The economically optimal operating light intensity for photocatalytic processes depends on the relative costs of the reactor and photon generation.[51] The optimal light power utilization, namely, quantum efficiency, is achieved in the first-order domain.[47] However, the application of LEDs can greatly reduce the cost of photon generation, so that increased intensity (below the mass-transfer-limited regime) can enhance the reaction rate per unit volume and is more economical.

3.5. Reaction Products and Possible Degradation Pathways. During the photocatalytic degradation experiments carried out at τ = 15 s, C_{in} = 3 ppmv, and I = 1.0 mW·cm^{-2}, reaction products released in the gas phase and adsorbed on the catalyst surface were identified. An overview of these reaction products together with the specific analytical techniques used is given in Table 3. There was no difference in the identification of the detected reaction products for the four types of LEDs, indicating that the photocatalytic degradation processes of DMS at λ > 350 nm have similar pathways. To the best of our knowledge, only a few studies have investigated the reaction products of DMS photocatalytic degradation. Possible reaction products include gaseous SO_2, CO_2 and, and oxidation intermediates such as dimethyl sulfoxide (DMSO), dimethyl sulfone ($DMSO_2$), and dimethyl disulfide (DMDS), as well as carbonyl acids and sulfate ion, absorbed on the catalyst surface.[9,28,53] Compared with these results, our study identified methanethiol (MT) in gas phase as a newly detected product, which was confirmed by the GC-FPD retention time and mass spectrometry analysis using the same method with a Varian VF-wax capillary column. Consequently, based on the detected reaction products listed in Table 3 and literature data,[9,28,54] photocatalytic degradation pathways of DMS under LED illumination are proposed.

As shown in Figure 7, DMS degradation is preceded by the adsorption of gaseous DMS onto the TiO_2 surface and the generation of electron−hole pairs (h^+−e^-) in the photon-induced catalyst. Heterogeneous photocatalytic oxidation processes can generate reactive oxygen species (ROS), such as hydroxyl radical ($^{\bullet}OH$), superoxide radical ($^{\bullet}O_2^-$), and H_2O_2.[8] ROS and h^+ can initiate the oxidation of surface-adsorbed DMS by two major pathways: S oxidation and C−S bond cleavage. The S-atom oxidation pathway is indicated by the identification of sulfate ion adsorbed on the catalyst surface. The S atom in a DMS molecule can be oxidized by $^{\bullet}OH$ radical to form DMSO and $DMSO_2$. Further attack by $^{\bullet}OH$ radical can result in the release of methyl radicals and the complete mineralization of sulfur as sulfate. The direct splitting of the C−S bond in DMS is made evident by the formation of DMDS and methanethoil (MT). The direct oxidation of DMS by h^+ can form dimethyl sulfinium radical, which is prone to split into a methyl sulfide radical and a methyl cation. Dimerization of methyl sulfide radical forms DMDS. Hydrogen peroxide and methyl sulfide radical can form

Table 3. Overview of Reaction Products Detected in the Gas Phase and Accumulated on the Catalyst Surface and the Analytical Techniques Employed

reaction product	formula	analytical technique[a]
	Gas Phase	
dimethyl sulfoxide (DMSO)	$(CH_3)_2SO$	SPME−GC−MS (HP-5MS)
dimethyl sulfone ($DMSO_2$)	$(CH_3)_2SO_2$	SPME−GC−MS (HP-5MS)
dimaethyl disulfide (DMDS)	$(CH_3)_2S_2$	SPME−GC−MS (HP-5MS)
methanethoil (MT)	CH_3SH	GC-FPD, SPME−GC−MS (VF-wax)
	Surface	
sulfate	SO_4^{2-}	IC-CD
methanesulfonic acid (MSA)	CH_3SO_3H	IC-CD

[a] GC-FPD, gas chromatography with flame photometric detection; IC-CD, ion chromatography with conductivity detection; SPME−GC−MS, solid-phase microextraction−gas chromatography−mass spectrometry.

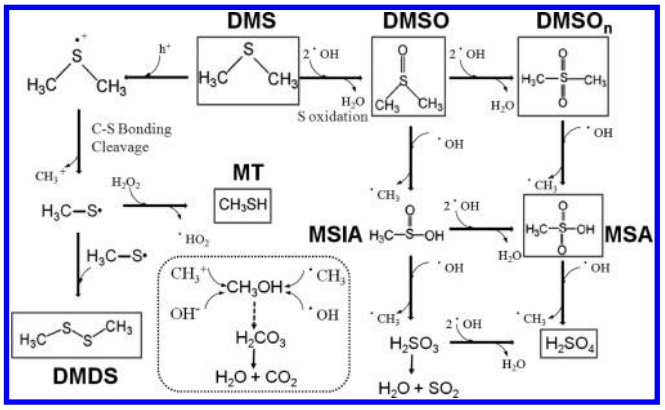

Figure 7. Plausible degradation pathways for the photocatalytic degradation of DMS on TiO_2 under 350−400-nm irradiation. Detected products are highlighted by solid rectangular boxes. Possible mineralization pathways of carbon are depicted separately in the dashed box, with the dashed arrow indicating multiple reaction steps that were omitted. Abbreviations: DMDS = dimethyl disulfide, DMS = dimethyl sulfide, DMSO = dimethyl sulfoxide, $DMSO_2$ = dimethyl sulfone, MSA = methanesulfonic acid, MSIA = methanesulfinic acid, and MT = methanethiol.

methanethiol.[55] Methanethoil was also recently detected in similar advanced oxidation process of DMS in the presence of ozone and TiO_2-based catalyst.[27] Methanethiol and DMDS can decompose by further C−S cleavage and S oxidation steps, in which methyl sulfide radical serves as an important intermediate.[33] The released methyl and hydroxyl radicals or ions can form methanol, which can be further oxidized to formaldehyde and formic acid and completely mineralized as carbon dioxide.

4. CONCLUSIONS

This study has demonstrated that the LED/TiO_2 photocatalytic process is a feasible deodorization technique. Among the four types of LEDs tested, 365- and 375-nm LEDs showed significantly superior abatement performance. The kinetics of DMS photocatalytic degradation could be modeled by the Langmuir−Hinshelwood rate law. The reaction rate depends on both the LED wavelength and intensity. The wavelength effect was attributed to the photon absorption property of the catalyst. The influence of light intensity on the reaction rate followed a nonlinear power law. The 365- and 375-nm LEDs showed a transition of the kinetic order with respect to light intensity at 0.5−1.0 mW·cm^{-2}, whereas the other two LEDs did not. The identification of the reaction products suggested C−S cleavage and S oxidation as the two degradation pathways of DMS under irradiation at the wavelengths (λ > 350 nm) investigated in this study.

AUTHOR INFORMATION

Corresponding Author

*E-mail: zhangsc@fudan.edu.cn (S.Z.), jmchen@fudan.edu.cn (J.C.). Tel.: +86-21-6564-2297 (S.Z.), +86-21-6564-2298 (J.C.).

Present Addresses

[†]Department of Energy, Environmental and Chemical Engineering, Washington University, St. Louis, MO 63130, United States.

Author Contributions

[‡]These authors contributed equally to this work.

ACKNOWLEDGMENT

This work was supported by the Natural Science Foundation of Shanghai (#07ZR14005), the Scientific Research Foundation for Returned Overseas Chinese Scholars (State Education Ministry), and the Century Star Program of Fudan University. Z.W. thanks the support from Fudan's Undergraduate Research Opportunities Program (FDUROP). The valuable comments and suggestions of the anonymous reviewers were helpful to improve the quality of this manuscript.

REFERENCES

(1) Lomans, B.; Smolders, A.; Intven, L.; Pol, A.; Op Den Camp, H.; Van Der Drift, C. Formation of dimethyl sulfide and methanethiol in anoxic freshwater sediments. *Appl. Environ. Microbiol.* **1997**, *63*, 4741–4747.

(2) Bentley, R.; Chasteen, T. G. Environmental VOSCs—Formation and degradation of dimethyl sulfide, methanethiol and related materials. *Chemosphere* **2004**, *55*, 291–317.

(3) Jäppinen, P.; Kangas, J.; Silakoski, L.; Savolainen, H. Volatile metabolites in occupational exposure to organic sulfur compounds. *Arch. Toxicol.* **1993**, *67*, 104–106.

(4) Devai, I.; DeLaune, R. D. Emission of reduced malodorous sulfur gases from wastewater treatment plants. *Water Environ. Res.* **1999**, *71*, 203–208.

(5) Torén, K.; Hagberg, S.; Westberg, H. Health effects of working in pulp and paper mills: Exposure, obstructive airways diseases, hypersensitivity reactions, and cardiovascular diseases. *Am. J. Ind. Med.* **1996**, *29*, 111–122.

(6) Estrada, J. M.; Kraakman, N. J. R. B.; Muñoz, R. l.; Lebrero, R. A Comparative Analysis of Odor Treatment Technologies in Wastewater Treatment Plants. *Environ. Sci. Technol.* **2010**, *45*, 1100–1106.

(7) Barton, J. W.; Klasson, K. T.; Koran, J. L. J.; Davison, B. H. Microbial Removal of Alkanes from Dilute Gaseous Waste Streams: Kinetics and Mass Transfer Considerations. *Biotechnol. Prog.* **1997**, *13*, 814–821.

(8) Hoffmann, M. R.; Martin, S. T.; Choi, W.; Bahnemann, D. W. Environmental applications of semiconductor photocatalysis. *Chem. Rev.* **1995**, *95*, 69–96.

(9) Demeestere, K.; Dewulf, J.; De Witte, B.; Van Langenhove, H. Titanium dioxide mediated heterogeneous photocatalytic degradation of gaseous dimethyl sulfide: Parameter study and reaction pathways. *Appl. Catal. B* **2005**, *60*, 93–106.

(10) Liu, T. X.; Li, X. Z.; Li, F. B. Development of a photocatalytic wet scrubbing process for gaseous odor treatment. *Ind. Eng. Chem. Res.* **2010**, *49*, 3617–3622.

(11) Li, X. Z.; Hou, M. F.; Li, F. B.; Chua, H. Photocatalytic oxidation of methyl mercaptan in foul gas for odor control. *Ind. Eng. Chem. Res.* **2006**, *45*, 487–494.

(12) Mo, J. H.; Zhang, Y. P.; Xu, Q. J.; Lamson, J. J.; Zhao, R. Y. Photocatalytic purification of volatile organic compounds in indoor air: A literature review. *Atmos. Environ.* **2009**, *43*, 2229–2246.

(13) Chen, D. H.; Ye, X.; Li, K. Oxidation of PCE with a UV LED photocatalytic reactor. *Chem. Eng. Technol.* **2005**, *28*, 95–97.

(14) Wang, W. Y.; Ku, Y. Photocatalytic degradation of Reactive Red 22 in aqueous solution by UV-LED radiation. *Water Res.* **2006**, *40*, 2249–2258.

(15) Chen, H. W.; Ku, Y.; Irawan, A. Photodecomposition of *o*-cresol by UV-LED/TiO_2 process with controlled periodic illumination. *Chemosphere* **2007**, *69*, 184–190.

(16) Chen, H. W.; Ku, Y.; Wu, C. Y. Effect of LED optical characteristics on temporal behaviour of *o*-cresol decomposition by UV/TiO_2 process. *J. Chem. Technol. Biotechnol.* **2007**, *82*, 626–635.

(17) Tayade, R. J.; Natarajan, T. S.; Bajaj, H. C. Photocatalytic degradation of methylene blue dye using ultraviolet light emitting diodes. *Ind. Eng. Chem. Res.* **2009**, *48*, 10262–10267.

(18) Gorges, R.; Meyer, S.; Kreisel, G. Photocatalysis in microreactors. *J. Photochem. Photobiol. A* **2004**, *167*, 95–99.

(19) Loetscher, L. H.; Carey, J. M.; Skiles, S. L.; Carey, V. M.; Boyd, J. E. Titania—acrylic coil reactor for photocatalytic water purification and sterilization. *Ind. Eng. Chem. Res.* **2009**, *48*, 4697–4702.

(20) Chatterley, C.; Linden, K. Demonstration and evaluation of germicidal UV-LEDs for point-of-use water disinfection. *J. Water Health* **2010**, *8*, 479–486.

(21) Ghosh, J. P.; Langford, C. H.; Achari, G. Characterization of an LED based photoreactor to degrade 4-chlorophenol in an aqueous medium using coumarin (C-343) sensitized TiO_2. *J. Phys. Chem. A* **2008**, *112*, 10310–10314.

(22) Ghosh, J. P.; Sui, R.; Langford, C. H.; Achari, G.; Berlinguette, C. P. A comparison of several nanoscale photocatalysts in the degradation of a common pollutant using LEDs and conventional UV light. *Water Res.* **2009**, *43*, 4499–4506.

(23) Qiu, R. L.; Zhang, D. D.; Mo, Y. Q.; Song, L.; Brewer, E.; Huang, X. F.; Xiong, Y. Photocatalytic activity of polymer-modified ZnO under visible light irradiation. *J. Hazard. Mater.* **2008**, *156*, 80–85.

(24) Izadifard, M.; Langford, C. H.; Achari, G. Photocatalytic dechlorination of PCB 138 using leuco-methylene blue and visible light; reaction conditions and mechanisms. *J. Hazard. Mater.* **2010**, *181*, 393–398.

(25) Izadifard, M.; Langford, C. H.; Achari, G. Photocatalytic dechlorination of polychlorinated biphenyls using leuco-methylene blue sensitization, broad spectrum visible lamps, or light emitting diodes. *Environ. Sci. Technol.* **2010**, *44*, 9075–9079.

(26) Shie, J.-L.; Lee, C.-H.; Chiou, C.-S.; Chang, C.-T.; Chang, C.-C.; Chang, C.-Y. Photodegradation kinetics of formaldehyde using light sources of UVA, UVC and UVLED in the presence of composed silver titanium oxide photocatalyst. *J. Hazard. Mater.* **2008**, *155*, 164–172.

(27) Sahle-Demessie, E.; Devulapelli, V. G. Vapor phase oxidation of dimethyl sulfide with ozone over V_2O_5/TiO_2 catalyst. *Appl. Catal. B* **2008**, *84*, 408–419.

(28) González-García, N.; Ayllón, J. A.; Doménech, X.; Peral, J. TiO_2 deactivation during the gas-phase photocatalytic oxidation of dimethyl sulfide. *Appl. Catal. B* **2004**, *52*, 69–77.

(29) Zhang, S.; Zheng, Z.; Wang, J.; Chen, J. Heterogeneous photocatalytic decomposition of benzene on lanthanum-doped TiO_2 film at ambient temperature. *Chemosphere* **2006**, *65*, 2282–2288.

(30) Biard, P. F.; Bouzaza, A.; Wolbert, D. Photocatalytic degradation of two volatile fatty acids in an annular plug-flow reactor; Kinetic modeling and contribution of mass transfer rate. *Environ. Sci. Technol.* **2007**, *41*, 2908–2914.

(31) Doucet, N.; Bocquillon, F.; Zahraa, O.; Bouchy, M. Kinetics of photocatalytic VOCs abatement in a standardized reactor. *Chemosphere* **2006**, *65*, 1188–1196.

(32) Imoberdorf, G. E.; Irazoqui, H. A.; Cassano, A. E.; Alfano, O. M. Photocatalytic degradation of tetrachloroethylene in gas phase on TiO_2 films: A kinetic study. *Ind. Eng. Chem. Res.* **2005**, *44*, 6075–6085.

(33) Yin, F.; Grosjean, D.; Seinfeld, J. H. Photooxidation of dimethyl sulfide and dimethyl disulfide. I: Mechanism development. *J. Atmos. Chem.* **1990**, *11*, 309–364.

(34) Qiao, L.; Chen, J.; Yang, X. Potential particulate pollution derived from UV-induced degradation of odorous dimethyl sulfide. *J. Environ. Sci. (China)* **2011**, *23*, 51–59.

(35) Talrose, V.; Stern, E. B.; Goncharova, A. A.; Messineva, N. A.; Trusova, N. V.; Efimkina, M. V.; Yermakov, A. N.; Usov, A. A.; Leskin, A. A. UV/visible spectra. In *NIST Chemistry WebBook*; NIST Standard Reference Database Number 69; National Institute of Standards and Technology: Gaithersburg, MD, 2008.

(36) Jacoby, W. A.; Blake, D. M.; Noble, R. D.; Koval, C. A. Kinetics of the oxidation of trichloroethylene in air via heterogeneous photocatalysis. *J. Catal.* **1995**, *157*, 87–96.

(37) Roupp, G. B.; Nico, J. A.; Annangi, S.; Changrani, R.; Annapragada, R. Two-flux radiation-field model for an annular packed-bed photocatalytic oxidation reactor. *AIChE J.* **1997**, *43*, 792–801.

(38) Salvadó-Estivill, I.; Hargreaves, D. M.; Li Puma, G. Evaluation of the intrinsic photocatalytic oxidation kinetics of indoor air pollutants. *Environ. Sci. Technol.* **2007**, *41*, 2028–2035.

(39) Wang, K.-H.; Tsai, H.-H.; Hsieh, Y.-H. The kinetics of photocatalytic degradation of trichloroethylene in gas phase over TiO_2 supported on glass bead. *Appl. Catal. B* **1998**, *17*, 313–320.

(40) Yamazaki-Nishida, S.; Nagano, K. J.; Phillips, L. A.; Cervera-March, S.; Anderson, M. A. Photocatalytic degradation of trichloroethylene in the gas phase using titanium dioxide pellets. *J. Photochem. Photobiol. A* **1993**, *70*, 95–99.

(41) Obee, T. N.; Hay, S. O. Effects of moisture and temperature on the photooxidation of ethylene on titania. *Environ. Sci. Technol.* **1997**, *31*, 2034–2038.

(42) Fox, M. A.; Dulay, M. T. Heterogeneous photocatalysis. *Chem. Rev.* **1993**, *93*, 341–357.

(43) Kim, S. B.; Hong, S. C. Kinetic study for photocatalytic degradation of volatile organic compounds in air using thin film TiO_2 photocatalyst. *Appl. Catal. B* **2002**, *35*, 305–315.

(44) Alberici, R. M.; Jardim, W. F. Photocatalytic destruction of VOCs in the gas-phase using titanium dioxide. *Appl. Catal. B* **1997**, *14*, 55–68.

(45) Palau, J.; Penya-Roja, J. M.; Gabaldón, C.; Javier Álvarez-Hornos, F.; Sempere, F.; Martínez-Soria, V. UV photocatalytic oxidation of paint solvent compounds in air using an annular TiO_2-supported reactor. *J. Chem. Technol. Biotechnol.* **2011**, *86*, 273–281.

(46) Vincent, G.; Marquaire, P. M.; Zahraa, O. Abatement of volatile organic compounds using an annular photocatalytic reactor: Study of gaseous acetone. *J. Photochem. Photobiol. A* **2008**, *197*, 177–189.

(47) Herrmann, J. M. Heterogeneous photocatalysis: State of the art and present applications. *Top. Catal.* **2005**, *34*, 49–65.

(48) Puddu, V.; Choi, H.; Dionysiou, D. D.; Puma, G. L. TiO_2 photocatalyst for indoor air remediation: Influence of crystallinity, crystal phase, and UV radiation intensity on trichloroethylene degradation. *Appl. Catal. B* **2010**, *94*, 211–218.

(49) Obee, T. N.; Brown, R. T. TiO_2 photocatalysis for indoor air applications: Effects of humidity and trace contaminant levels on the oxidation rates of formaldehyde, toluene, and 1,3-butadiene. *Environ. Sci. Technol.* **1995**, *29*, 1223–1231.

(50) Yu, H. L.; Zhang, K. L.; Rossi, C. Theoretical study on photocatalytic oxidation of VOCs using nano-TiO_2 photocatalyst. *J. Photochem. Photobiol. A* **2007**, *188*, 65–73.

(51) Ollis, D. F.; Pelizzetti, E.; Serpone, N. Photocatalyzed destruction of water contaminants. *Environ. Sci. Technol.* **1991**, *25*, 1522–1529.

(52) Rincón, A. G.; Pulgarin, C. Photocatalytical inactivation of *E. coli*: Effect of (continuous−intermittent) light intensity and of (suspended−fixed) TiO_2 concentration. *Appl. Catal. B* **2003**, *44*, 263–284.

(53) Nishikawa, H.; Takahara, Y. Adsorption and photocatalytic decomposition of odor compounds containing sulfur using TiO_2/SiO_2 bead. *J. Mol. Catal. A: Chem.* **2001**, *172*, 247–251.

(54) Vorontsov, A. V.; Savinov, E. N.; Lion, C.; Smirniotis, P. G. TiO_2 reactivation in photocatalytic destruction of gaseous diethyl sulfide in a coil reactor. *Appl. Catal. B* **2003**, *44*, 25–40.

(55) Turnipseed, A. A.; Barone, S. B.; Ravishankara, A. R. Reaction of OH with dimethyl sulfide. 2. Products and mechanisms. *J. Phys. Chem.* **1996**, *100*, 14703–14713.